Food Chemistry: X 24 (2024) 101922

Contents lists available at ScienceDirect

Food Chemistry: X

journal homepage: www.sciencedirect.com/journal/food-chemistry-x

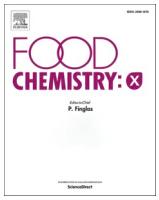

Application potential of wheat bran cellulose nanofibers as Pickering emulsion stabilizers and stabilization mechanisms

Jiawu Wu [a,b,c], Yang Gao [a,b,c], Huifang Shen [a,b,c], Song Yan [a,b,c], Rui Zhao [a,b,c], Fei Wang [a,b,c], Xinting Shen [a,b,c], Zhebin Li [a,b,c], Xinmiao Yao [a,b,c,*], Yao Wang [a,b,c,*]

[a] Food Processing Research Institute, Heilongjiang Academy of Agricultural Sciences, Harbin 150086, China
[b] Heilongjiang Province Key Laboratory of Food Processing, Harbin 150086, China
[c] Heilongjiang Province Engineering Research Center of Whole Grain Nutritious Food, Harbin 150086, China

ARTICLE INFO

Keywords:
Wheat bran
Cellulose nanofiber
Pickering emulsion

ABSTRACT

In this paper, cellulose nanofibers (CNF) were prepared from wheat bran (WB) and the structure of CNF was determined. Fourier transform infrared spectra and X-ray diffractograms showed the groups such as hydroxyl and carboxyl groups and cellulose type 1 structure possessed by CNF, respectively. Scanning electron microscopy exhibited that CNF was filamentous and intertwined. In addition, Pickering emulsions were prepared using CNF and the physicochemical properties of the emulsions were characterized. The results showed that CNF was able to increase the zeta potential and viscosity of the emulsions, thus improving the stability of the emulsions. Moreover, CNF formed a physical barrier by adsorbing at the oil-water interface and near the oil droplets and CNF dispersed in the aqueous phase formed a network structure to restrict the movement of oil droplets, thus improving the stability of the emulsions. These findings may provide some new insights for the potential applications of WB.

1. Introduction

Cellulose is the most dominant and widely distributed carbohydrate polymer on earth. Due to its low cost, biodegradability, non-toxicity and compatibility, it is receiving increasing attention (Gao et al., 2023). When cellulose is subjected to mechanical treatments, such as high-pressure homogenization and ultrasound, the cellulose fibres are disassembled into nanoscale structures, preserving the crystalline and amorphous regions, often described as CNF (Parajuli & Urena-Benavides, 2022). CNF is a nanoscale cellulose material, typically with diameters of 1–100 nm and lengths of a few micrometers. Depend on the high aspect ratio and the amphiphilic surface properties of CNF, making it a high quality material to stabilize food emulsions (Fang, Tian, Cai, et al., 2024). Ling Zhang et al. (2024a); Zhang et al. (2024b) isolated CNF from mushroom rhizomes and prepared a semi-solid emulsion with good stability. Lv et al. employed CNF and nano-chitin to synergistically stabilize high internal phase Pickering emulsions and exhibited high tolerance to salt ions and pH (Lv, Wang, et al., 2024). In addition, the use of CNF to stabilize essential oil emulsions can improve the stability of essential oils during use and maintain their antibacterial activity (Chevalier et al., 2024).

Moreover, CNF is available from a wide range of sources, including plants, bacteria and fungi (Czaikoski et al., 2020). But due to the increasing demand for sustainable food products, a large number of low value-added bioresources (such as banana peels, manzanita stalks and Oil palm fruit bunch) have been utilized for CNF production (Q. Li et al., 2021). And developing these resources can improve the technical and profit potential of these low value-added materials. Among these resources, agricultural resources have lower lignin content compared to woody biomass, and therefore require less chemicals and energy consumption during extraction. Thus, agricultural residues (such as bagasse, corn stover and rice straw) have become an excellent raw material for cellulose owing to their low cost and sustainability, and the extraction of CNF from agricultural residues has received increasing attention (Ji & Wang, 2023). Among the common agricultural crops, wheat is the most widely grown crop in the world with an annual production of more than 770 million tonnes. The bread and noodles using wheat as an ingredient are a major part of the human diet (Z. Chen,

* Corresponding authors.
E-mail addresses: cocoyococo@163.com (X. Yao), wang1221yao1221@163.com (Y. Wang).

https://doi.org/10.1016/j.fochx.2024.101922
Received 31 July 2024; Received in revised form 17 October 2024; Accepted 22 October 2024
Available online 28 October 2024

Mense, et al., 2024). Furthermore, the main by-product of wheat processing is WB, which has an average fiber content of 37–52 % and is highly promising for applications (Paesani et al., 2024). However, limited by a number of technical, functional and organoleptic challenges, WB is often used for animal feed development or rural fuel, or even discarded outright, lacking value-added applications (He et al., 2023a; He et al., 2023b). Therefore, though WB is rich in cellulose, current researches on WB are mainly focused on the functional properties and physicochemical properties of WB arabinoxylan. Yan et al. found that high molecular weight WB arabinoxylan could hinder starch pasting and low molecular WB arabinoxylan could inhibit starch degradation, thus improving the quality of starch products (W. Yan et al., 2022). WB arabinoxylan feruloylation also significantly increased the viscoelasticity of gluten and the quality of wheat products (Liu, Zhang, et al., 2023). Additionally, some studies have been conducted on the functional activity of WB and WB cellulose as dietary fiber. Zhong et al. found that nanosized WB insoluble dietary fiber had a better ability to inhibit starch and lipid digestion (Zhong et al., 2024). He et al. observed that WB insoluble dietary fiber inhibited starch digestion by decreasing the activity of α-Amylase using in vitro digestion experiments (He et al., 2023a; He et al., 2023b). In contrast, the means of application and development of WB cellulose are relatively homogeneous and these resources cannot be fully utilized. Nevertheless, large molecules like cellulose have the potential to be the emulsion stabilizer. And the application of cellulose from WB in emulsions has not been systematically investigated. Therefore, the preparation of CNF from WB cellulose to stabilize Pickering emulsions fills a gap in its application in emulsions. This also improves the utilization and development of WB cellulose and contributes to the high value utilization of WB.

Thus, this study aims to stabilize Pickering emulsions using WB CNF and investigate the stabilization mechanism. The structure of CNF was characterized using Fourier transform infrared (FTIR) spectroscopy, X-ray diffraction (XRD), scanning electron microscopy (SEM) and thermogravimetric (TGA) analysis. The particle size, zeta potential, creaming index (CI) and rheological properties of the emulsions prepared from CNF were determined. In addition, the distribution of CNF in the emulsions was analysed using fluorescence microscopy to explore the potential mechanism for CNF to stabilize Pickering emulsions. These results could provide some ideas and theoretical support for potential applications of WB and other agricultural wastes.

2. Materials and methods

2.1. Materials

Sodium hydroxide, sodium chlorite, 2,2,6,6-tetramethylpiperidine oxide (TEMPO) and sodium hypochlorite solutions were purchased from Shanghai Macklin Biochemical Technology Co Ltd. (Shanghai, China). WB was obtained from a local supermarket. Sodium dodecyl sulfate (SDS) and sodium bromide were provided by Shanghai Yuanye Biotechnology Co. (Shanghai, China). Medium-chain triglyceride (MCT) was bought from Sports Research Co. (San Pedro, CA, USA). Calcofluor White Stain was obtained from Beijing Coolaber Technology Co. (Beijing, China). Nile red dye was purchased from Aladdin Chemical Reagents (Shanghai, China). In this work, all other chemical reagents used were analytically pure.

2.2. Preparation of CNF

CNF was prepared according to the methods of Tang et al. and Xiao et al. with slight modifications (Tang et al., 2024; Xiao et al., 2023). Firstly, the WB was dried for crushing and then washed using ethanol for 12 h to remove the lipids. The defatted WB sample was mixed (1:20) with 5 % (*w/v*) sodium hydroxide solution and reacted at 70 °C for 4 h. Subsequently, the insoluble residue was mixed with a 1.5 % (w/v) sodium chlorite solution and the pH of the whole system was adjusted to 3–4 for the bleaching treatment. The bleaching treatment was repeated four times. The bleached sample was washed repeatedly with distilled water to pH neutral and freeze-dried to obtain wheat bran cellulose (WBC). The dried WBC was mixed with distilled water (1:100) and 0.008 g of TEMPO and 0.08 g of NaBr were added to react for 15 min. Then 7.5 mL of NaClO solution was added slowly and the pH of the whole reaction system was adjusted to 11 with NaOH solution and HCl solution. The whole reaction lasted for 5 h. At the end of the reaction, ethanol was added to terminate the reaction. Then the prepared oxidized cellulose sample was washed repeatedly with distilled water until the supernatant was neutral. Finally, CNF sample was obtained after treating the oxidized cellulose for 30 min (750 W) using an ultrasonic processor.

2.3. Zeta potential and particle size

The particle size and zeta potential of WBC and CNF were determined using a Zeta potential and particle size analyser (90Plus PALS, Brookhaven Instruments Inc., USA). The sample suspension (0.1 %) was prepared using deionised water, while the sample suspension was diluted by 100 times before measurement to avoid multiple scattering effects (Wang, Huang, et al., 2024).

2.4. FTIR spectroscopy

The sample powder was mixed with KBr and pressed into tablets and FTIR spectrum was determined by using a Nicolet iS50 FTIR spectrometer (Thermo Fisher Scientific, Waltham, MA, USA). The FTIR spectra of WB, WBC and CNF were obtained after 32 scans at the range of 400–4000 cm^{-1} (Ebrahimi et al., 2024a; Ebrahimi et al., 2024b).

2.5. XRD

Firstly, 100 mg of WB, WBC and CNF samples were taken on glass slides. Then the XRD patterns of WB,WBC and CNF samples were obtained after scanning in the range of 10–40° at a rate of 5°/min by a D8 X-ray diffractometer (Bruker, Germany) (Zhimao Li et al., 2023).

2.6. TGA

The TGA curves of WB,WBC and CNF were recorded by using TGA2 TGA analyser (Mettler Toledo, Switzerland). A 20 mg sample powder was taken in the TGA analyser and heated from room temperature to 600 °C at a rate of 10°/min under nitrogen atmosphere (Zhou, Lv, et al., 2024).

2.7. SEM

The morphology of WB,WBC and CNF was observed by using a scanning electron microscope (SU1510, Hitachi, Japan). A 5 mg sample powder was applied uniformly on the conductive adhesive tape and then the sample was observed under an accelerating voltage of 10 kV after gold spraying treatment (Tang, Hu, Bai, et al., 2024).

2.8. Preparation of Pickering emulsions

The oil-in-water Pickering emulsion was prepared using CNF suspension as the aqueous phase and MCT as the oil phase. The prepared CNF suspensions with different concentrations were mixed with MCT in the ratio of 3:1 and homogenised using a high speed homogeniser at 12000 rpm for 5 min. Finally, the Pickering emulsions were obtained with a concentration of MCT of 25 % and final concentrations of CNF of 0.2 %,0.4 %, 0.6 %, 0.8 % and 1 %, respectively.

2.9. Emulsifying activity index (EAI) and emulsion stability index (ESI)

The EAI and ESI were measured based on the method of Wang et al. with slight modifications (Wang, Liu, et al., 2024). Firstly, the emulsion was prepared using the method of 2. 8 and then 20 μL of the emulsion was removed from the bottom of the emulsion at 0 min and 60 min, respectively. Subsequently, 20 μL of the emulsion was diluted 100 times using 0.1 % SDS (*w/v*) and the absorbance value was measured at 500 nm by a UV-2450 spectrophotometer (Shimadzu, Tokyo, Japan). Finally, the EAI and ESI were calculated according to Eqs. (1) and (2):

$$EAI\left(\frac{m^2}{g}\right) = \frac{2 \times 2.303 \times A_0 \times N}{(1-\varphi) \times C \times 10000} \quad (1)$$

$$ESI\ (\%) = \frac{A_{60}}{A_0} \times 100 \quad (2)$$

where A_0 is the absorbance value at 0 min, N is the dilution times, φ is the volume fraction of the oil phase, C is the concentration of the sample, and A_{60} is the absorbance value at 60 min.

2.10. Characterization of emulsions

2.10.1. Zeta potential and particle size

The prepared emulsion was diluted 100 times using deionised water. The zeta potential and particle size of the emulsions were evaluated at 25 °C with a particle size analyser (90Plus PALS, Brookhaven Instruments Inc., USA) (Luo et al., 2024).

2.10.2. Rheological properties

A 2 mL of emulsion was placed on the sample stage and then the emulsion was sheared at a range of 0.01–100 s^{-1} using a DHR-2 rheometer (TA Instruments Inc., USA) equipped with parallel plates. The parallel plates were spaced 0.5 mm apart and the test temperature was 25 °C (Zhou, Feng, et al., 2024).

2.10.3. Microstructure observation

The distribution of CNF and oil droplets in the emulsions was observed using a DMi8 fluorescence microscope (Leica Microsystems, Germany). A 0.1 % Nile red (*w/v*) solution was mixed with 0.1 % calcofluor white (w/v) at a ratio of 1:1. Then 10 μL of the mixed dye was added to 1 mL of the prepared emulsion for staining. Finally the microstructure of the emulsion was observed in fluorescence mode (Taha et al., 2019).

2.10.4. CI

A 8 mL of the prepared emulsion was placed in a glass vial and kept sealed at room temperature for 20 days (Krstonošić et al., 2024). The height of the transparent layer at the bottom of the emulsion was measured every 4 days and changes of the emulsion were recorded. CI was calculated according to the following equation:

$$CI\ (\%) = \frac{H_s}{H_t} \times 100 \quad (3)$$

where H_s is the height of the transparent layer at the bottom of the emulsion and H_t is the total height of the emulsion.

2.10.5. Thermal stability

Thermal stability was determined using the emulsion stabilized by 1 % CNF and the emulsion stabilized by 1 % soybean protein isolate (SPI) was used as a control. The emulsion samples of 5 mL were placed in a water bath and heated at 50 °C, 60 °C, 70 °C, 80 °C and 90 °C for 30 min. The treated samples were cooled down to room temperature and then left to stand for 2 h. Finally, the zeta potentials, average particle sizes and microstructures of the emulsions were determined (Tang, Wang, Li, et al., 2024).

2.10.6. Salt ion stability

Salt ion stability was determined using the emulsion stabilized with 1 % CNF and the emulsion stabilized with 1 % SPI was used as a control. The emulsion samples were mixed in equal volumes with different molar concentrations of NaCl, making the final concentrations of NaCl in the emulsions into 50 mM, 100 mM, 150 mM, 200 mM, and 300 mM, respectively. The zeta potentials, average particle sizes, and microstructures of the emulsions were recorded after 2 h of resting time (Wang, Bu, et al., 2024).

2.11. Statistical analysis

Origin 2024 (OriginLab, Northampton, MA, USA) was used to plot the graphs. The data were statistically analysed using IBM SPSS statistical software (version 24.0, SPSS, INC., Chicago, IL, USA) and one-way analysis of variance (ANOVA). All samples were measured three times and the results were expressed as mean ± standard deviation. The Duncan's multiple range test was used to determine significant differences between samples ($p < 0.05$).

3. Results and discussion

3.1. Zeta potential and particle size

The zeta potential, average particle size and PDI of WBC and CNF are shown in Table 1. Compared to WBC, the absolute value of zeta potential was significantly increased in CNF. The significant change in zeta potential is mainly attributed to the large number of carboxyl groups introduced during TEMPO oxidation (Alizade et al., 2024). Moreover, ultrasound treatment can shear micron-sized cellulose to form nanosized CNF, which results in the average particle size of CNF being significantly smaller than the WBC (Lin, Yang, Kong, et al., 2024a). In addition, CNF showed a narrower particle size distribution (Fig. 1A) and lower PDI compared to WBC. This may be due to the homogeneity of CNF promoted by TEMPO oxidation (Tang, Wang, Bai, et al., 2024). Jiang et al. also showed a more concentrated particle size distribution of CNF of bamboo shoots after TEMPO oxidation treatment (Jiang et al., 2024).

3.2. FTIR analysis

The FTIR spectra of the samples are shown in Fig. 1B. In general, the peak at 893 cm^{-1} represents the bending vibration of the C—H bond (Zhe Li et al., 2024). The peaks at 1105 cm^{-1} and 1155 cm^{-1} are attributed to the glycosidic ether bond of C-O-C and the ring breathing of C—C, respectively. These two bands can indicate the cellulose content in WB, WBC and CNF (Abbasi et al., 2024). The intensity of the peak at 1105 cm^{-1} was significantly higher in WBC and CNF than in WB. This is mainly attributed to the removal of lignin and hemicellulose during alkali treatment and bleaching. Moreover, the peaks at 1318 cm^{-1} and 1368 cm^{-1} represent the parent chains of the cellulose molecule (Ebrahimi et al., 2024a; Ebrahimi et al., 2024b). Similarly, the peaks in these two bands were significantly stronger in WBC and CNF than in WB. In addition, the peak at 1545 cm^{-1} may indicate a vibration of the C═C aromatic backbone in lignin (Ebrahimi et al., 2024a; Ebrahimi et al., 2024b). With the removal of lignin, this peak largely disappeared in WBC and CNF. In all samples, a broad peak corresponding to the stretching vibration of the -OH group appeared near 3300 cm^{-1}. However, the intensity of the peak near 3300 cm^{-1} in CNF decreased, a peak corresponding to the sodium carboxylate group appeared at 1612 cm^{-1}

Table 1
Zeta potential, average particle size and PDI of WBC and CNF.

	Zeta potential (mV)	Average particle size (nm)	PDI
WBC	−21.36 ± 2.74	2582.18 ± 321.23	0.62 ± 0.06
CNF	−53.46 ± 2.26	522.58 ± 83.57	0.46 ± 0.07

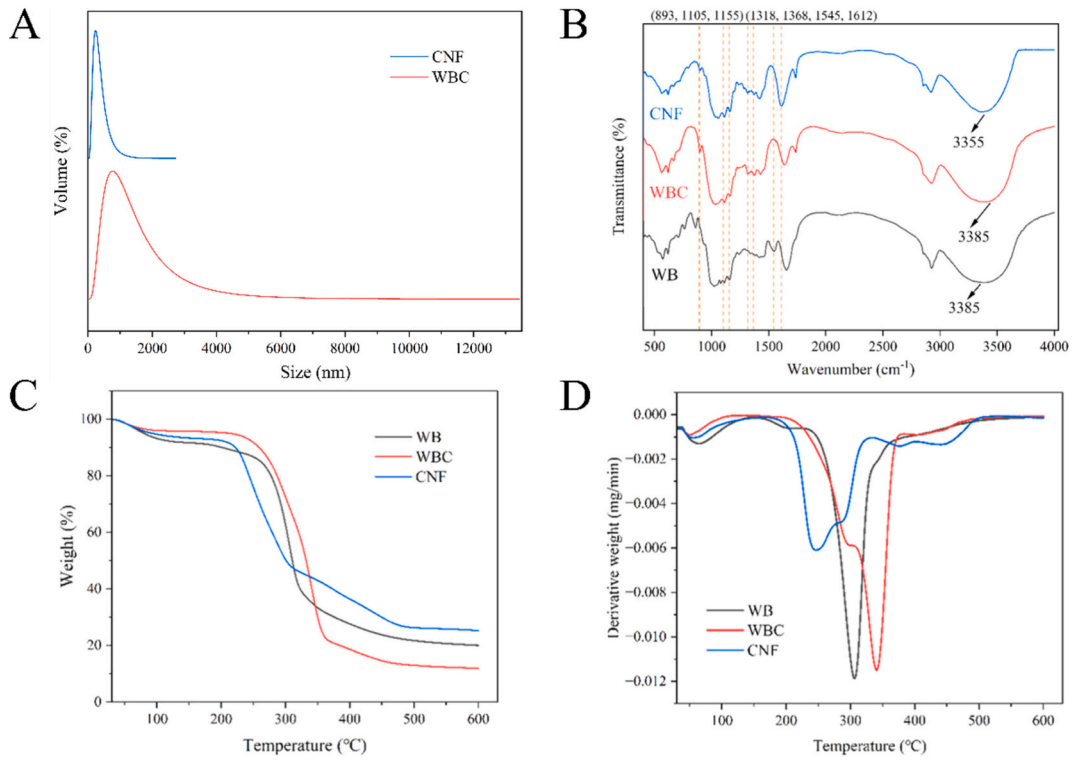

Fig. 1. Particle size distribution (A) of WBC and CNF. FTIR spectra (B), TGA (C) and DTG (D) curves of WB,WBC and CNF.

at the same time. This is due to the oxidation of the -OH group on the surface of cellulose to -COONa under alkaline conditions (Jiaying Zhu et al., 2024). Piao et al. also found that the FTIR spectra of TEMPO oxidized cellulose showed an oxidatively formed C = O stretching peak at 1600 cm^{-1} (Piao et al., 2022).

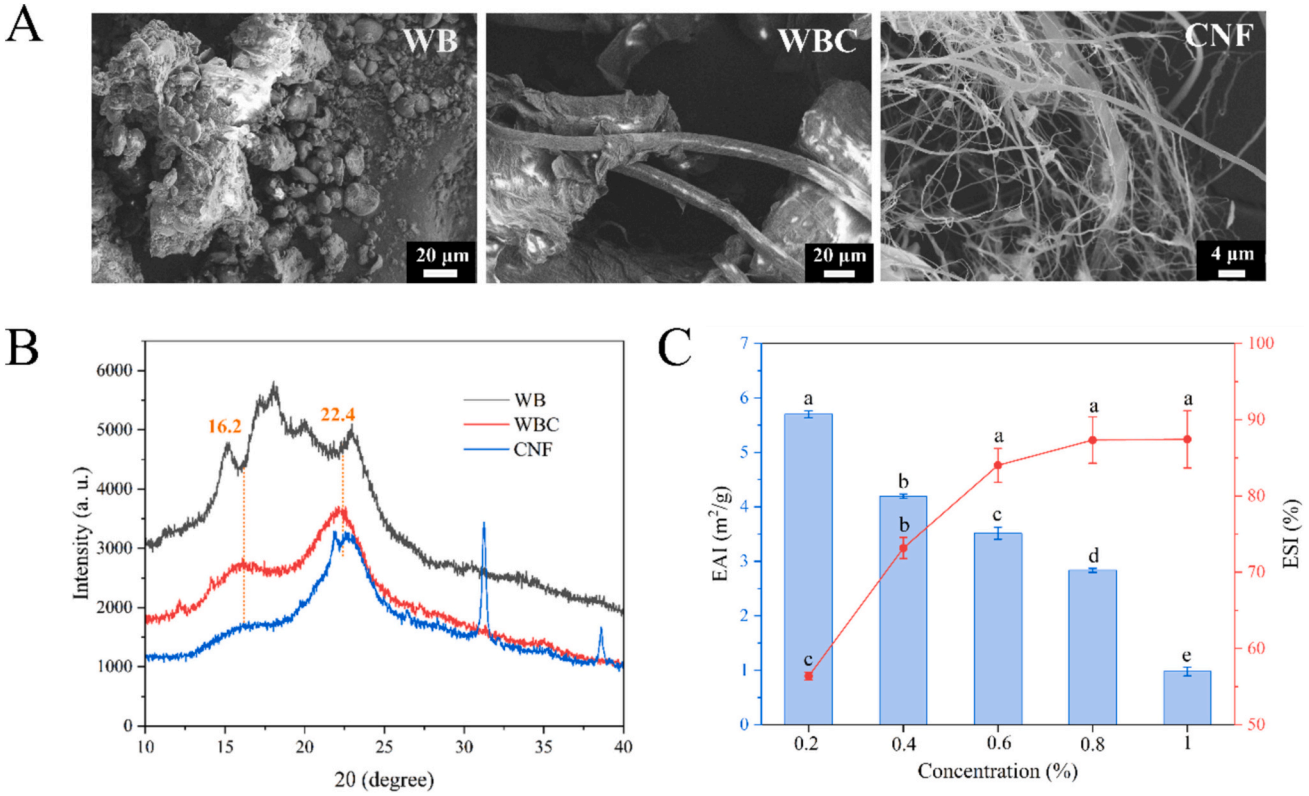

Fig. 2. SEM images (A) and XRD patterns (B) of WB,WBC and CNF. EAI and ESI (C) of different concentrations of CNF. Different letters indicate significant differences ($p < 0.05$).

3.3. TGA analysis

The thermal stability of the samples was analysed using TGA and derivative thermogravimetric (DTG) curves. The results are shown in Fig. 1C and Fig. 1D. All the samples showed a slow phase of weight loss between 30 °C -150 °C. This is mainly attributed to the evaporation of water (Zhong et al., 2024). In addition, the maximum degradation of both WBC and CNF was lower than the WB as observed by the DTG and TGA curves. The maximum degradation of WB, WBC and CNF corresponded to temperatures of 306.333 °C, 340.5 °C and 246.333 °C, respectively. This is mainly due to the lignin and hemicellulose in WB being more readily degraded and at lower degradation temperatures compared to cellulose (Xiao et al., 2019). Bhupender et al. also reported that cellulose materials containing lignin were more easily degradable (Mahur et al., 2023). This is also the reason why the maximum degradation temperature of WB is lower than that of WBC. Moreover, during the TEMPO oxidation process, the increase of oxidation contributed to a decrease in the degree of cellulose polymerisation, thus leading to a rapid depolymerisation and decomposition of cellulose at 246.333 °C in CNF. And the high surface area of CNF exposes its surface more to heat, leading to the lower thermal stability than WB and WBC (Kurd et al., 2024).

3.4. XRD analysis

The crystal structure of the samples was analysed using XRD and the XRD patterns of the different samples are shown in Fig. 2B. As seen in the figure, there were two characteristic diffraction peaks at 16.2° and 22.4° for both WBC and CNF, corresponding to the cellulose type 1 structure in the cellulose sample (Wu et al., 2024). According to the study, the cellulose type 1 structure has stronger hydrophobic interactions and contributes to the stability of Pickering emulsions (Dai et al., 2020). In contrast, WB only had a broad peak between 15°-25° which could come from the amorphous part. This was consistent with the results of Quan et al. (Quan et al., 2024). And there was a significant increase in the intensity of the major crystalline peaks at 22.4° for WBC and CNF compared to WB, which were attributed to purification processes such as alkali treatment and bleaching.

3.5. SEM analysis

The SEM images of the samples are shown in Fig. 2A. Large numbers of spherical particles and lumpy structures appeared in the image of WB. This is mainly starch and protein present in the WB. And during the crushing process, the starch and proteins were mixed to form large lumpy structures (Mouzakitis et al., 2024). After alkali treatment and bleaching, smooth-surfaced rhizomatous fibrous structures have emerged in WBC compared to WB. This is mainly due to the removal of the non-cellulose fraction such as lignin. In addition, flat and dense laminar fibrous structures were found in the WBC (Saini et al., 2023). In contrast, CNF was separated from the original fiber bundles after TEMPO and ultrasound treatments, showing a significant reduction in diameter and a distinct filamentous structure (Lin, Yang, Kong, et al., 2024a). This also presented a similar structure to the CNF of potato residue separated using ultrasound combined with high pressure homogenization by Liu et al. (X. Liu, Sun, et al., 2023).

3.6. EAI and ESI

The emulsifying ability of CNF and the ability to keep the emulsion from delamination were analysed using EAI and ESI (Huang et al., 2021). As shown in Fig. 2C, the EAI gradually decreased with the increase of CNF concentration. This may be due to the fact that CNF lacks hydrophobic groups such as propyl itself, resulting in a low adsorption rate and adsorption capacity of CNF at the oil-water interface. Lin et al. also reported the increase in the concentration of citrus peel nanocellulose leading to a decrease of surface hydrophobicity (Lin, Yang, Qi, et al., 2024). As the concentration of CNF increased, the hydrophilicity of CNF was further strengthened, and the emulsifying ability of CNF on the oil phase was weakened, which could not sufficiently emulsify the oil droplets (Usurelu et al., 2024).

Compared to EAI, ESI was positively correlated with the concentration of CNF. This is related to the structure of the CNF itself. With the increase of CNF concentration, the more particles adsorbed on the surface of oil droplets, the CNF will spontaneously kink and entangle to form a thicker interfacial layer in the vicinity of the oil droplets, preventing the aggregation and fusion between the oil droplets (Qin et al., 2023a). Therefore, the increase in CNF concentration improved the stability of the emulsion, leading to an increase in ESI.

3.7. Zeta potential and particle size of emulsions

Particle size and size distribution are often used to describe the degree of aggregation of droplets in emulsions, and zeta potential is used to characterise the magnitude of electrostatic attraction or repulsion between droplets, which are closely related to the stability of emulsion systems (Jianyu Zhu et al., 2023). The particle size and zeta potential of the emulsions prepared with different CNF concentrations are shown in Fig. 3A. As the increase of CNF concentration, the absolute value of zeta potential of the emulsion gradually increased. When the CNF concentration was 1 %, the zeta potential of the emulsion was −53 mV, at which time the strong electrostatic repulsion between the emulsion droplets helped to maintain the stability of the emulsion. Furthermore, the rise in the absolute value of the emulsion zeta potential is mainly due to the increase in the concentration of carboxyl groups. Since CNF contains a large number of carboxyl groups, the increase in CNF content leads to the higher surface charge density and absolute value of zeta potential of the emulsion (C. Yan et al., 2023). However, the emulsion particle size gradually increased with the rise of CNF concentration. This showed opposite results to previous studies on CNF-stabilized Pickering emulsions. The reason for this result may be the spontaneous binding of CNF into aggregates through hydrogen bonding interactions, leading to agglomeration of CNF and contributing to the increase of emulsion particle size (Usurelu et al., 2024).

Additionally, the particle size distributions of the emulsions are shown in Fig. 3B. The particle size distributions of the emulsions stabilized with 0.2 % and 0.4 % CNF were mainly concentrated below 2000 nm. As the concentration further increased, the particle size distribution peak of the emulsions also showed a significant rightward shift. This also presented the same trend with the average particle size of the emulsions.

3.8. Rheological properties of emulsions

The viscosity of emulsions prepared by different concentrations of CNF is shown in Fig. 3C. Along with the increase of shear rate, all samples showed shear thinning. The fluid properties of emulsions are usually influenced by the interactions between emulsifier molecules in the continuous phase (Chen, Li, et al., 2024). Consequently, under stress of shear, the fiber network structure of the CNF breaks into individual fibres, which are usually aligned along the direction of flow, leading to a decrease in the viscosity of the continuous phase and shear thinning of the emulsion (Fang, Tian, Huang, et al., 2024). In addition, as shown in Fig. 3C, the viscosity of the emulsion was positively correlated with the concentration of CNF. On the one hand, an increase in CNF content reduces the distance between individual fibres, encouraging them to contact and entangle with each other to form a dense cellulose network, which prevents the flow of emulsion droplets and increases the viscosity of the emulsion (Y. Liu, Shi, et al., 2023). Shang et al. also reported that CNF improved the viscosity of emulsions by promoting the formation of a three-dimensional network structure (Shang et al., 2023). On the other hand, CNF contains a large number of polar groups such as carboxyl and hydroxyl groups, providing it with a strong hydrophilicity and ability to

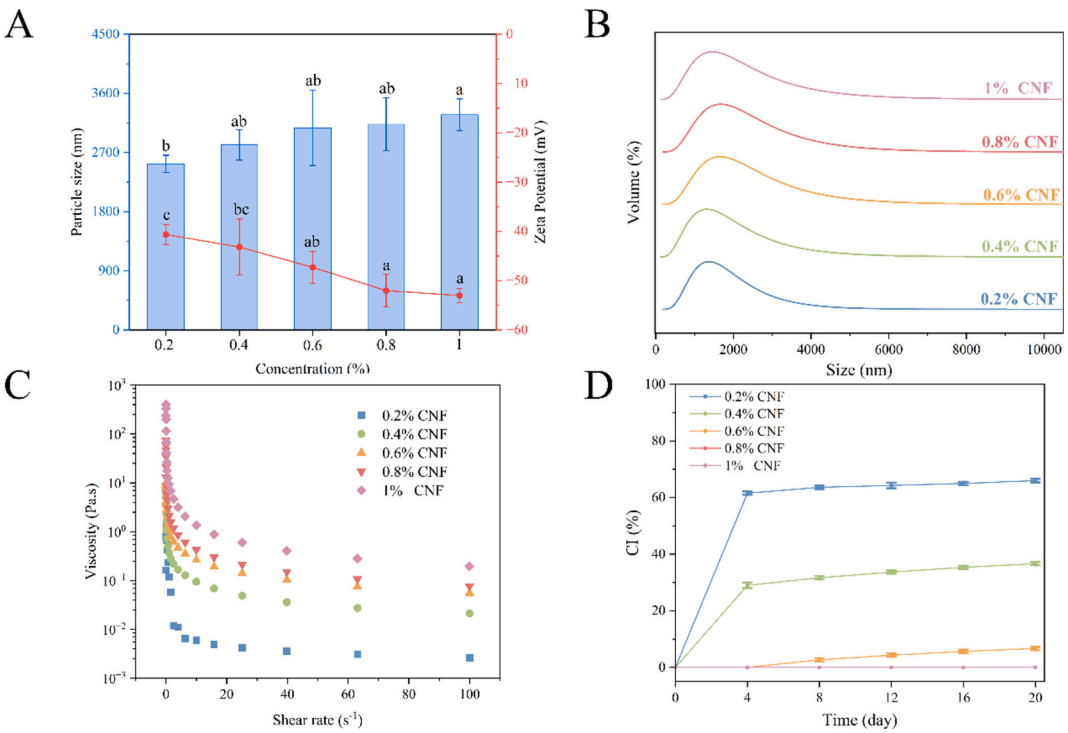

Fig. 3. Zeta potential, average particle size (A), particle size distribution (B), rheological properties (C) and CI (D) of emulsions prepared with different concentrations of CNF. Different letters indicate significant differences ($p < 0.05$).

bind water. This will make the mobility of the water molecules in the emulsion decrease and the viscosity of the emulsion increase (Dong et al., 2022).

3.9. Microstructure of emulsions

To further investigate the underlying mechanism of the stabilization of Pickering emulsions by CNF, the distribution of oil droplets and CNF in the emulsions was observed using fluorescence microscopy. Fluorescence microscopy images of emulsions stabilized with different concentrations of CNF are shown in Fig. 4A. When the CNF content was 0.2 %, there was only a small amount of CNF adsorbed at the oil-water interface and on the surface of oil droplets, and some CNF was dispersed in the continuous phase. Therefore, 0.2 % CNF could not

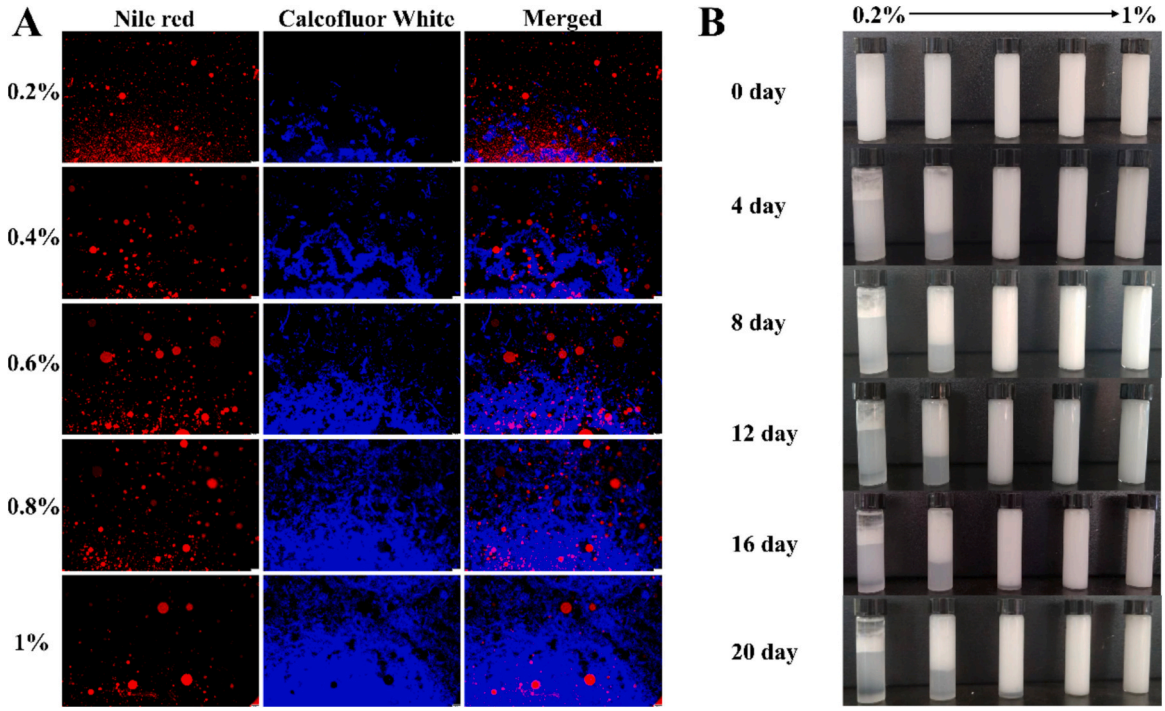

Fig. 4. Fluorescence microscope pictures (A) and appearance (B) during storage of emulsions prepared with different concentrations of CNF.

effectively cover the oil droplets and entangle in the continuous phase to form an extensive interlocking cellulose network, thus inhibiting the aggregation of oil droplets (Uşurelu et al., 2024). In addition, when the concentration of CNF reached 0.6 % or more, a large amount of CNF covered the surface of oil droplets to form an interfacial barrier, preventing the aggregation and fusion between oil droplets (Tan et al., 2024). Meanwhile, the long and flexible CNF spontaneously bonded and entangled by hydrogen bonds to form a viscous cellulose network in the continuous phase (R. Guo et al., 2024). And the strong cellulose network formed by CNF can act as a physical barrier to hinder the movement and aggregation of oil droplets, thus improving the stability of the emulsion. Cui et al. also recorded that high concentrations of nanocellulose could completely form a continuous network through van der waals forces and hydrogen bonds interactions, allowing oil droplets to be uniformly captured (Cui et al., 2023). Thus, high concentration of CNF can effectively improve the stability of emulsion. This result also shows the same trend as that of ESI.

3.10. CI of emulsions

Storage stability of emulsions is an important factor affecting the shelf life of emulsions in food applications. CI is commonly used to evaluate the stability of emulsions during storage (Wang, Lin, et al., 2024). The CI of the emulsions prepared by different concentrations of CNF is shown in Fig. 3D. The CI of the emulsions prepared with 0.2 %, 0.4 % and 0.6 % CNF increased with time. According to the appearance pictures of the emulsions (Fig. 4B), the emulsions prepared with 0.2 % and 0.4 % CNF showed creaming in 4–20 days, while the emulsions prepared with 0.6 % CNF presented only slight creaming in 16–20 days. The upper layer exhibited a milky layer and the lower layer was transparent. This may be because the relatively low concentration of CNF cannot be sufficiently adsorbed on the surface of the oil droplets, and the small amount of CNF dispersed in the continuous phase fails to provide sufficient electrostatic repulsion, leading to the occurrence of creaming. In addition, the emulsions stabilized with 0.8 % and 1 % CNF both showed a CI of 0 for 0–20 days, and their emulsion appearance also displayed a homogeneous milky white colour with no phase separation (Fig. 4B). On the one hand, emulsions prepared by 0.8 % and 1 % CNF have a high viscosity. This will inhibit the movement of oil droplets and prevent their aggregation and fusion (Phosanam et al., 2023). On the other hand, the high concentration of CNF tends to form an ordered cellulose network in the continuous phase and provides a strong electrostatic repulsion to prevent the proximity of oil droplets to each other, thus improving the stability of the emulsion (Lv, Zou, et al., 2024). Similarly, Qin et al. also found that bacterial nanocellulose oxidized by TEMPO prevented the aggregation of oil droplets by adsorbing at the oil-water interface, resulting in emulsions without creaming after 15 days of storage (Qin et al., 2023b).

3.11. Thermal stability of emulsions

As shown in Fig. 5A, the 1 % CNF-stabilized emulsion showed an increase in average particle size after heating, but there was no significant change in average particle size with increasing temperature. The microscope pictures of the emulsions also showed a slight aggregation and fusion of the oil droplets after heating, but there was no significant change in the state of the droplets as the temperature increased (Fig. 5B).

This is mainly attributed to the cellulose network structure formed by CNF entanglement that limits the movement and aggregation of oil droplets, promoting better thermal stability of CNF-stabilized emulsions (Lin, Yang, Kong, et al., 2024b). In addition, the absolute value of the zeta potential of the CNF-stabilized emulsions decreased after heating, but no significant decrease in the absolute value of the zeta potential of the emulsions was observed when they were heated from 50 °C to 90 °C. And at different temperatures, the absolute value of zeta potential of CNF-stabilized emulsions was higher than 44 mV, indicating strong electrostatic repulsion between emulsion droplets at this time to maintain the stability of the emulsions. This also presented similar results to the study by Chen et al. (S. Chen et al., 2023).

In contrast, the 1 % SPI-stabilized emulsion showed a significant increase in mean particle size when heated to 50 °C. This may be due to SPI thermal denaturation leading to reduced solubility and hence formation of aggregates (Sun et al., 2022). Interestingly, the average particle size of the emulsions showed a decreasing trend from 60 °C to 90 °C (Fig. 5C). With the increase of temperature, the hydrophobic amino acids inside the SPI are exposed, resulting in higher surface activity and EAI of the SPI at the oil-water interface. This result is confirmed by the weakening of aggregation between oil droplets when heated to 90 °C (Fig. 5D). More oil droplets are covered by the SPI, reducing the particle size of the emulsion (Ma et al., 2022). Moreover, the absolute value of

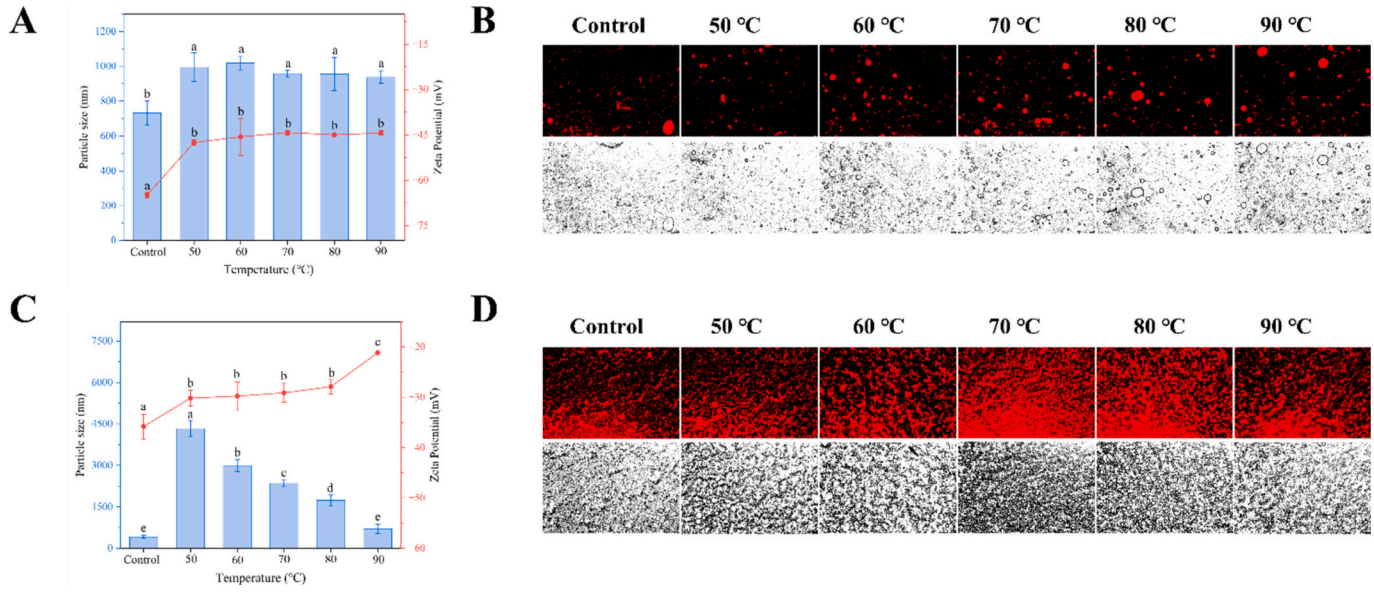

Fig. 5. Average particle size and zeta potential of CNF-stabilized (A) and SPI-stabilized (C) emulsions at different temperatures. Microstructure of CNF-stabilized (B) and SPI-stabilized (D) emulsions at different temperatures. Oil phase was stained red using Nile Red. Different letters indicate significant differences ($p < 0.05$). (For interpretation of the references to colour in this figure legend, the reader is referred to the web version of this article.)

the zeta potential of the emulsions gradually decreased with increasing temperature, indicating that the SPI-stabilized emulsions had lower thermal stability compared to CNF.

3.12. Salt ion stability of emulsions

As shown in Fig. 6A, the average particle size of CNF-stabilized emulsions was positively correlated with NaCl concentration. It can also be seen from the microscope images that the oil droplets of the emulsions with NaCl were aggregated and fused to form larger oil droplets compared to the control group (Fig. 6B). In contrast, the SPI-stabilized emulsions showed a more substantial increase in average particle size with increasing NaCl concentration (Fig. 6C). Significant aggregation between droplets also occurred compared to the control group (Fig. 6D). This is all related to the electrostatic shielding effect produced by Na^+. The large amount of Na^+ neutralises the negative charges carried by CNF and SPI, leading to a weakening of the electrostatic repulsion between emulsion droplets and aggregation of droplets (Zhao, Chang, et al., 2024). The decrease in the absolute value of the zeta potential of emulsions stabilized by CNF and SPI confirms this reason.

3.13. Mechanism of stabilization of Pickering emulsions by WB CNF

The potential mechanism of WB CNF to stabilize the Pickering emulsion is shown in Fig. 7. Firstly, CNF is adsorbed to the oil-water interface to form Pickering emulsions. In one aspect, Low concentrations of CNF (under 0.6 %) cannot completely cover the oil droplets and form a strong physical barrier around the droplets to inhibit droplet aggregation. In contrast, high concentrations of CNF (0.6 % and above) are adsorbed on the surface and around the oil droplets, thus forming a thicker interfacial layer around the droplets and preventing them from agglomerating. On the other hand, low concentrations of CNF are unable to form an effective cellulose network in the continuous phase and can only exist in a fragmented form. High concentrations of CNF can spontaneously bind in the continuous phase and form a dense three-dimensional network structure between the oil droplets to inhibit the free movement and fusion of the oil droplets (Zhang et al., 2024a; Zhang et al., 2024b).

Besides, CNF has the property of changing the viscosity of the aqueous phase of the emulsion. High concentrations of CNF tend to overlap and link together to form entangled networks and macrogels that can act as thickeners in aqueous media at low concentrations, thus contributing to emulsion stability (S. Guo et al., 2022). Moreover, the generation of very high viscosity and gelatinous behaviour of the medium is able to trap a continuous phase between the droplets in the network, thus inhibiting creaming of the emulsion (Szlapak Franco et al., 2020). Meanwhile, the increase of CNF concentration enhances the structure of the continuous phase and forms larger aggregates. The adsorption energy of the aggregates is greater than the repulsive force between CNF and the oil-water interface, enabling CNF to adsorb to the oil-water interface more easily to stabilize the emulsion. Pinto et al. found a similar phenomenon in their study on the stabilization of Pickering emulsions by bacterial nanocellulose (Pinto et al., 2024).

Furthermore, from the optical microscope picture in Fig. 7, a large number of elongated CNF were dispersed among the emulsion, while the droplets were distributed around the CNF. This reveals that the CNF may act as continuous anchors to regulate the distribution of droplets in the emulsion. These structures can prevent the aggregation and fusion of droplets, thus improving the stability of the emulsion. Zhao et al. also reported that TEMPO oxidized nanocellulose could stabilize the emulsion by forming this special anchoring structure (Zhao, Zhang, et al., 2024).

4. Conclusions

CNF from WB was prepared by TEMPO oxidation and ultrasonication. Zeta potential and FTIR results indicated that the hydroxyl groups of cellulose were successfully oxidized to carboxylic acid groups. TGA showed that the thermal stability of CNF was reduced. The prepared CNF was found to be filamentous and entangled by SEM, and the cellulose type 1 structure of CNF suggested the potential advantage of stabilization of Pickering emulsions. In addition, Pickering emulsions were prepared using CNF and the stability of the emulsions was characterized. Finally, it was found that CNF was able to adsorb on the surface and around the oil droplets to provide a strong electrostatic repulsion, preventing proximity of the oil droplets. The unadsorbed CNF present in the continuous phase then entangled with each other to form a strong cellulose network structure, thus limiting the free movement of the emulsion droplets to aggregate. Moreover, the CNF could connect in the aqueous phase to form entangled networks and gels to increase the viscosity of the aqueous phase, thus inhibiting creaming and phase

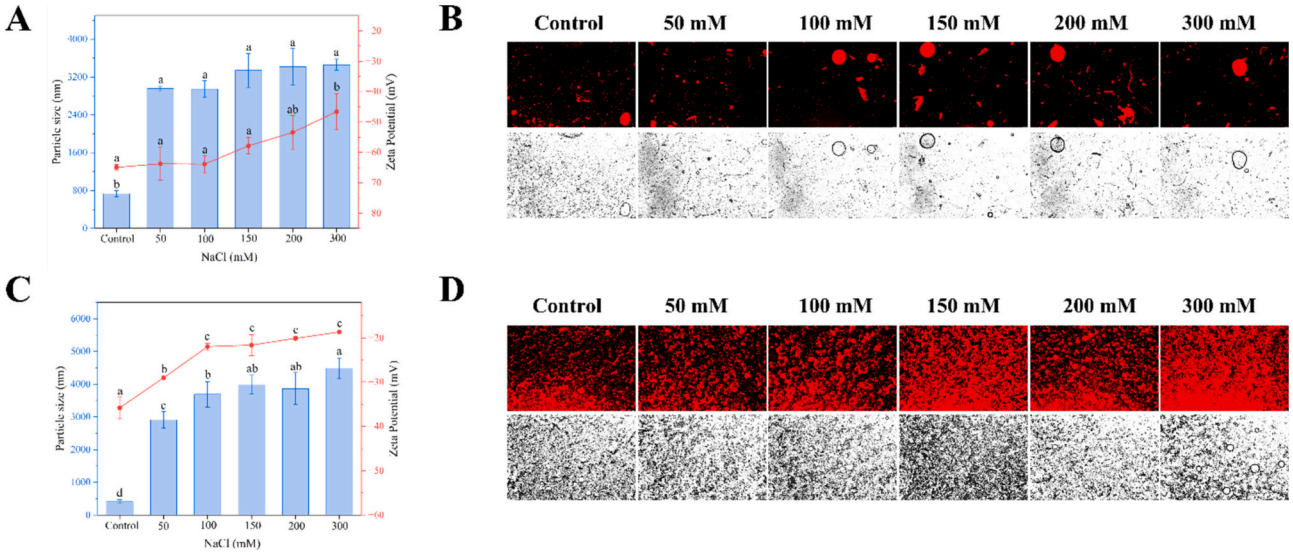

Fig. 6. Average particle size and zeta potential of CNF-stabilized (A) and SPI-stabilized (C) emulsions at different ion concentrations. Microstructure of CNF-stabilized (B) and SPI-stabilized (D) emulsions at different ion concentrations. Oil phase was stained red using Nile Red. Different letters indicate significant differences ($p < 0.05$). (For interpretation of the references to colour in this figure legend, the reader is referred to the web version of this article.)

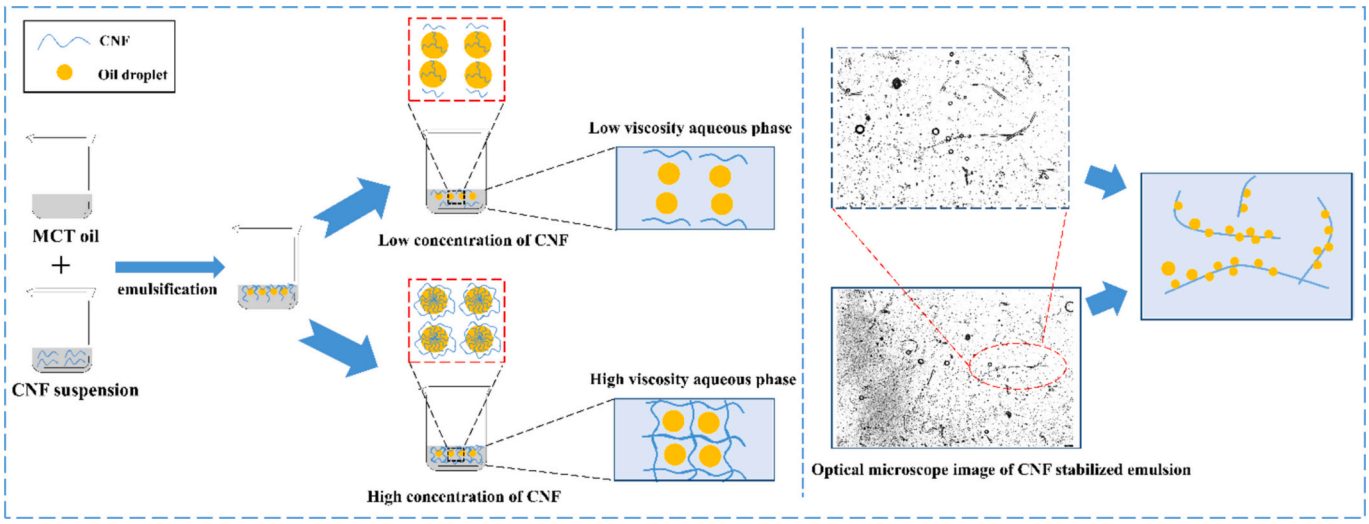

Fig. 7. Mechanism diagram of WB CNF to stabilize Pickering emulsion.

separation of the emulsions and further improving the stability of the emulsions. It was worth mentioning that CNF-stabilized emulsions also showed excellent thermal and ionic stability. These results may provide some new ideas for the high value utilization of WB and offer theoretical guidance for the application of CNF from other agricultural waste sources in emulsions. However, this study only evaluated the effect of WB CNF on the stability of low oil-phase Pickering emulsions and lacked the study of WB CNF in medium and high internal phase Pickering emulsions. This limits the application of WB CNF in the food industry to some extent. Future research should focus on the stabilizing ability of WB CNF for higher oil phase emulsions.

CRediT authorship contribution statement

Jiawu Wu: Writing – original draft. **Yang Gao:** Investigation. **Huifang Shen:** Software, Resources. **Song Yan:** Data curation. **Rui Zhao:** Validation. **Fei Wang:** Formal analysis. **Xinting Shen:** Visualization. **Zhebin Li:** Methodology. **Xinmiao Yao:** Methodology, Conceptualization. **Yao Wang:** Writing – review & editing.

Declaration of competing interest

The authors declare that they have no known competing financial interests or personal relationships that could have appeared to influence the work reported in this paper.

Data availability

Data will be made available on request.

Acknowledgments

This work was supported by the Research funding for scientific research institutes in Heilongjiang Province (CZKYF2023-1-B030).

References

Abbasi, A., Makhtoumi, Y., Wu, Y., & Chen, G. (2024). Characterization of cellulose nanocrystal extracted from household waste and its application for seed germination. *Carbohydrate Polymer Technologies and Applications, 7*. https://doi.org/10.1016/j.carpta.2023.100409

Alizade, A., Reich, T., & Jantschke, A. (2024). Cellulose from dinoflagellates as a versatile and environmentally friendly platform for the production of functionalised cellulose nanofibres. *International Journal of Biological Macromolecules, 272*(Pt 1), Article 132804. https://doi.org/10.1016/j.ijbiomac.2024.132804

Chen, S., Lai, H., Su, X., Yu, H., Li, B., Wei, S., … Yue, P. (2023). Rambutan-liked Pickering emulsion stabilized by cellulose nanocrystals for enhancing anti-bacterial activity and anti-inflammatory effect of Chimonanthus nitens Oliv. Essential oil. *International Journal of Biological Macromolecules, 242*, Article 124665. https://doi.org/10.1016/j.ijbiomac.2023.124665

Chen, W., Li, X., Zhang, W., Alouk, I., Wang, Y., Xu, D., & Sun, B. (2024). Physicochemical properties, photostability, and digestive characteristics of natural emulsion system fabricated by recombinant rice bran oil bodies for lutein ester delivery. *Food Hydrocolloids, 156*, Article 110270. https://doi.org/10.1016/j.foodhyd.2024.110270

Chen, Z., Mense, A. L., Brewer, L. R., & Shi, Y.-C. (2024). Wheat bran arabinoxylans: Chemical structure, extraction, properties, health benefits, and uses in foods. *Comprehensive Reviews in Food Science and Food Safety, 23*(3), Article e13366. https://doi.org/10.1111/1541-4337.13366

Chevalier, R. C., Almeida, N. A., de Oliveira Rocha, L., & Cunha, R. L. (2024). Antimicrobial potential of oregano essential oil vehiculated in Pickering cellulose nanofibers-stabilized emulsions. *International Journal of Biological Macromolecules, 275*, Article 133457. https://doi.org/10.1016/j.ijbiomac.2024.133457

Cui, J., Hossain, M., Wang, Z., & Chang, C. (2023). Enzymatically produced nanocellulose as emulsifier for Pickering emulsion. *Food Hydrocolloids, 144*, Article 108997. https://doi.org/10.1016/j.foodhyd.2023.108997

Czaikoski, A., da Cunha, R. L., & Menegalli, F. C. (2020). Rheological behavior of cellulose nanofibers from cassava peel obtained by combination of chemical and physical processes. *Carbohydrate Polymers, 248*, Article 116744. https://doi.org/10.1016/j.carbpol.2020.116744

Dai, H., Wu, J., Zhang, H., Chen, Y., Ma, L., Huang, H., … Zhang, Y. (2020). Recent advances on cellulose nanocrystals for Pickering emulsions: Development and challenge. *Trends in Food Science & Technology, 102*, 16–29. https://doi.org/10.1016/j.tifs.2020.05.016

Dong, H., Li, Y., Jia, C., Zhang, B., Niu, M., Zhao, S., & Xu, Y. (2022). Mechanism behind the rheological property improvement of fava bean protein by the presence of dextran. *Food Hydrocolloids, 133*, Article 107907. https://doi.org/10.1016/j.foodhyd.2022.107907

Ebrahimi, R., Fathi, M., & Ghoddusi, H. B. (2024a). Pickering emulsions stabilized by cellulose nanocrystals extracted from hazelnut shells: Production and stability under different harsh conditions. *International Journal of Biological Macromolecules, 258*(Pt 2), Article 128982. https://doi.org/10.1016/j.ijbiomac.2023.128982

Ebrahimi, R., Fathi, M., & Ghoddusi, H. B. (2024b). Pickering emulsions stabilized by cellulose nanocrystals extracted from hazelnut shells: Production and stability under different harsh conditions. *International Journal of Biological Macromolecules, 258*, Article 128982. https://doi.org/10.1016/j.ijbiomac.2023.128982

Fang, F., Tian, Z., Cai, Y., Huang, L., Van der Meeren, P., & Wang, J. (2024). The structural, antioxidant and emulsifying properties of cellulose nanofiber-dihydromyricetin mixtures: Effects of composite ratio. *Food Chemistry, 454*, Article 139803. https://doi.org/10.1016/j.foodchem.2024.139803

Fang, F., Tian, Z., Huang, L., Cai, Y., Van der Meeren, P., & Wang, J. (2024). A novel Pickering emulsion gels stabilized by cellulose nanofiber/dihydromyricetin composite particles: Microstructure, rheological behavior and oxidative stability. *International Journal of Biological Macromolecules, 278*, Article 135281. https://doi.org/10.1016/j.ijbiomac.2024.135281

Gao, J., Qiu, Y., Chen, F., Zhang, L., Wei, W., An, X., & Zhu, Q. (2023). Pomelo peel derived nanocellulose as Pickering stabilizers: Fabrication of Pickering emulsions and their potential as sustained-release delivery systems for lycopene. *Food Chemistry, 415*, Article 135742. https://doi.org/10.1016/j.foodchem.2023.135742

Guo, R., Li, H., Liu, K., Xu, H., Wang, K., Yang, Z., … Wang, C. (2024). Processable Pickering emulsion for composite cryogel with cellulose nanofibrils and nanochitin. *Carbohydrate Polymers, 334*, Article 122034. https://doi.org/10.1016/j.carbpol.2024.122034

Guo, S., Bai, L., Li, J., Bi, R., Huan, S., & Rojas, O. J. (2022). Depletion effects and stabilization of Pickering emulsions prepared from a dual Nanocellulose system. *ACS Sustainable Chemistry & Engineering, 10*(28), 9066–9076. https://doi.org/10.1021/acssuschemeng.2c01059

He, T., Zhang, X., Zhao, L., Zou, J., Qiu, R., Liu, X., … Wang, K. (2023a). Insoluble dietary fiber from wheat bran retards starch digestion by reducing the activity of alpha-amylase. *Food Chemistry, 426*, Article 136624. https://doi.org/10.1016/j.foodchem.2023.136624

He, T., Zhang, X., Zhao, L., Zou, J., Qiu, R., Liu, X., … Wang, K. (2023b). Insoluble dietary fiber from wheat bran retards starch digestion by reducing the activity of alpha-amylase. *Food Chemistry, 426*, Article 136624. https://doi.org/10.1016/j.foodchem.2023.136624

Huang, Y., Zhang, D., Zhang, Y., Fang, H., & Zhou, C. (2021). Role of ultrasound and l-lysine/l-argnine in improving the physical stability of myosin-soybean oil emulsion. *Food Hydrocolloids, 111*. https://doi.org/10.1016/j.foodhyd.2020.106367

Ji, C., & Wang, Y. (2023). Nanocellulose-stabilized Pickering emulsions: Fabrication, stabilization, and food applications. *Advances in Colloid and Interface Science, 318*, Article 102970. https://doi.org/10.1016/j.cis.2023.102970

Jiang, Y., Lu, Y., Liu, J., Zhao, Y., & Fan, F. (2024). Characterization of bamboo shoot cellulose nanofibers modified by TEMPO oxidation and ball milling method and its application in W/O emulsion. *Lwt, 205*. https://doi.org/10.1016/j.lwt.2024.116563

Krstonošić, V., Pavlović, N., Nikolić, I., Milutinov, J., & Ćirin, D. (2024). Physicochemical properties and stability of oil-in-water emulsions stabilized by soy protein isolate and xanthan gum. *International Journal of Biological Macromolecules, 260*, Article 129610. https://doi.org/10.1016/j.ijbiomac.2024.129610

Kurd, F., Fathi, M., Shahedi, M., & Soltanizadeh, N. (2024). Aerogel composite based on cellulose nanofibril and poly vinyl alcohol as insulation for meat packaging. *Journal of Food Engineering, 367*, Article 111854. https://doi.org/10.1016/j.jfoodeng.2023.111854

Li, Q., Wu, Y., Fang, R., Lei, C., Li, Y., Li, B., … ShilinLiu.. (2021). Application of Nanocellulose as particle stabilizer in food Pickering emulsion: Scope, merits and challenges. *Trends in Food Science & Technology, 110*, 573–583. https://doi.org/10.1016/j.tifs.2021.02.027

Li, Z., Guan, J., Yan, C., Chen, N., Wang, C., Liu, T., … Shao, Z. (2023). Corn straw core/cellulose nanofibers composite for food packaging: Improved mechanical, bacteria blocking, ultraviolet and water vapor barrier properties. *Food Hydrocolloids, 143*, Article 108884. https://doi.org/10.1016/j.foodhyd.2023.108884

Li, Z., Liu, A., Wu, H., Naeem, A., Fan, Q., Jin, Z., … Ming, L. (2024). Extraction of cellulose nanocrystalline from Camellia oleifera Abel waste shell: Study of critical processes, properties and enhanced emulsion performance. *International Journal of Biological Macromolecules, 254*, Article 127890. https://doi.org/10.1016/j.ijbiomac.2023.127890

Lin, J., Yang, J., Kong, J., Shen, M., Yu, Q., Chen, Y., & Xie, J. (2024a). Effect of cellulose nanofibrils on stability and digestive properties of legume protein-based emulsions. *Food Hydrocolloids, 151*. https://doi.org/10.1016/j.foodhyd.2024.109779

Lin, J., Yang, J., Kong, J., Shen, M., Yu, Q., Chen, Y., & Xie, J. (2024b). Effect of cellulose nanofibrils on stability and digestive properties of legume protein-based emulsions. *Food Hydrocolloids, 151*, Article 109779. https://doi.org/10.1016/j.foodhyd.2024.109779

Lin, J., Yang, J., Qi, X., Shen, M., & Xie, J. (2024). Effect of cellulose nanofibrils on formation, interactions and gelation properties of chickpea protein isolate emulsion gels. *Food Hydrocolloids, 156*, Article 110252. https://doi.org/10.1016/j.foodhyd.2024.110252

Liu, A., Zhang, Y., Zhao, X., Li, D., Xie, C., Yang, R., … Wang, P. (2023). The role of feruloylation of wheat bran arabinoxylan in regulating the heat-evoked polymerization behavior of gluten. *Food Hydrocolloids, 134*, Article 108046. https://doi.org/10.1016/j.foodhyd.2022.108046

Liu, X., Sun, H., Mu, T., Fauconnier, M. L., & Li, M. (2023). Preparation of cellulose nanofibers from potato residues by ultrasonication combined with high-pressure homogenization. *Food Chemistry, 413*, Article 135675. https://doi.org/10.1016/j.foodchem.2023.135675

Liu, Y., Shi, Z., Zou, Y., Yu, J., Liu, L., & Fan, Y. (2023). Comparison of cellulose and chitin nanofibers on Pickering emulsion stability-investigation of size and surface wettability contribution. *International Journal of Biological Macromolecules, 235*, Article 123754. https://doi.org/10.1016/j.ijbiomac.2023.123754

Luo, Y., Yu, M., Liyixia, Z., & Chen, J. (2024). Effect of different pretreatment methods on the stability of pumpkin seed milk and potential mechanism. *Food Chemistry, 452*, Article 139582. https://doi.org/10.1016/j.foodchem.2024.139582

Lv, J., Wang, H., Zhu, M., Chen, Q., Huan, S., Liu, Y., … Bai, L. (2024). High internal phase Pickering emulsions via complexation of cellulose nanofibrils and nanochitin: Enhanced interfacial adsorption and structured aqueous network. *Food Hydrocolloids, 157*, Article 110383. https://doi.org/10.1016/j.foodhyd.2024.110383

Lv, J., Zou, C., Dai, Q., Zhao, Y., Zhu, M., Liu, X., … Bai, L. (2024). Pickering emulsions stabilized by aldehyde-modified cellulose nanofibrils: Stabilization and asphalt recovery application. *Industrial Crops and Products, 218*, Article 118967. https://doi.org/10.1016/j.indcrop.2024.118967

Ma, J., Chen, H., Chen, W., Wu, J., Li, Z., Zhang, M., … Chen, W. (2022). Effects of heat treatment and pH on the physicochemical and emulsifying properties of coconut (*Cocos nucifera* L.) globulins. *Food Chemistry, 388*, Article 133031. https://doi.org/10.1016/j.foodchem.2022.133031

Mahur, B. K., Ahuja, A., Singh, S., Maji, P. K., & Rastogi, V. K. (2023). Different nanocellulose morphologies (cellulose nanofibers, nanocrystals and nanospheres) extracted from Sunn hemp (crotalaria Juncea). *International Journal of Biological Macromolecules, 253*, Article 126657. https://doi.org/10.1016/j.ijbiomac.2023.126657

Mouzakitis, C.-K., Kotsiou, K., Pontikakos, G., Matzapetakis, M., Zervou, M., Biliaderis, C. G., & Lazaridou, A. (2024). Unravelling the structural heterogeneity and diversity in rheological behavior of alkali-extractable wheat bran arabinoxylans using ammonia pretreatment. *Food Hydrocolloids, 151*. https://doi.org/10.1016/j.foodhyd.2024.109888

Paesani, C., Lammers, T., Sciarini, L. S., Moiraghi, M., Perez, G. T., & Fabi, J. P. (2024). Effect of chemical, thermal, and enzymatic processing of wheat bran on the solubilization, technological and biological properties of non-starch polysaccharides. *Carbohydrate Polymers, 328*, Article 121747. https://doi.org/10.1016/j.carbpol.2023.121747

Parajuli, S., & Urena-Benavides, E. E. (2022). Fundamental aspects of nanocellulose stabilized Pickering emulsions and foams. *Advances in Colloid and Interface Science, 299*, Article 102530. https://doi.org/10.1016/j.cis.2021.102530

Phosanam, A., Moreira, J., Adhikari, B., Adhikari, A., & Losso, J. N. (2023). Stabilization of ginger essential oil Pickering emulsions by pineapple cellulose nanocrystals. *Current Research in Food Science, 7*, Article 100575. https://doi.org/10.1016/j.crfs.2023.100575

Piao, X., Li, J., Zhao, Y., Guo, L., Zheng, B., Zhou, R., & Ostrikov, K. (2022). Oxidized cellulose nanofibrils-based surimi gel enhancing additives: Interactions, performance and mechanisms. *Food Hydrocolloids, 133*, Article 107893. https://doi.org/10.1016/j.foodhyd.2022.107893

Pinto, N. O. F., Bourbon, A. I., Martins, D., Pereira, A., Cerqueira, M. A., Pastrana, L., … Gonçalves, C. (2024). Bacterial cellulose nanocrystals or nanofibrils as Pickering stabilizers in low-oil emulsions: A comparative study. *Food Hydrocolloids, 157*. https://doi.org/10.1016/j.foodhyd.2024.110427

Qin, X., Li, B., Li, L., Wang, F., Jia, S., Xie, Y., & Zhong, C. (2023a). Cinnamon essential oil Pickering emulsions: Stabilization by bacterial cellulose nanofibrils and applications for active packaging films. *Food Bioscience, 56*. https://doi.org/10.1016/j.fbio.2023.103258

Qin, X., Li, B., Li, L., Wang, F., Jia, S., Xie, Y., & Zhong, C. (2023b). Cinnamon essential oil Pickering emulsions: Stabilization by bacterial cellulose nanofibrils and applications for active packaging films. *Food Bioscience, 56*, Article 103258. https://doi.org/10.1016/j.fbio.2023.103258

Quan, W., Wang, J., Huang, J., & Zhang, D. (2024). Structure characterization and dye adsorption properties of modified Fiber from wheat bran. *Molecules, 29*(11), 2581. https://www.mdpi.com/1420-3049/29/11/2581.

Saini, P., Sinha, A. S. K., & Prasad, K. (2023). Wet refining: A novel approach for modification of wheat bran fiber. *Innovative Food Science & Emerging Technologies, 90*. https://doi.org/10.1016/j.ifset.2023.103508

Shang, X., Qiao, J., Chang, S., & Li, K. (2023). Effects of the addition sequence of soybean protein isolate and cellulose nanofibers on the properties and in vitro digestion of emulsions. *Lwt, 183*, Article 114897. https://doi.org/10.1016/j.lwt.2023.114897

Sun, Y., Chen, H., Chen, W., Zhong, Q., Zhang, M., & Shen, Y. (2022). Effects of ultrasound combined with preheating treatment to improve the thermal stability of coconut Milk by modifying the physicochemical properties of coconut protein. *Foods, 11*(7). https://doi.org/10.3390/foods11071042

Szlapak Franco, T., Martínez Rodríguez, D. C., Jiménez Soto, M. F., Jiménez Amezcua, R. M., Urquíza, M. R., Mendizábal Mijares, E., & de Muniz, G. I. B. (2020). Production and technological characteristics of avocado oil emulsions stabilized with cellulose nanofibrils isolated from agroindustrial residues. *Colloids and Surfaces A: Physicochemical and Engineering Aspects, 586*. https://doi.org/10.1016/j.colsurfa.2019.124263

Taha, A., Ahmed, E., Hu, T., Xu, X., Pan, S., & Hu, H. (2019). Effects of different ionic strengths on the physicochemical properties of plant and animal proteins-stabilized emulsions fabricated using ultrasound emulsification. *Ultrasonics Sonochemistry, 58*, Article 104627. https://doi.org/10.1016/j.ultsonch.2019.104627

Tan, Y., Wu, P., Yu, J., Bai, J., Nie, C., Liu, B., … Wang, J. (2024). Stabilization of Pickering emulsions with bacterial cellulose nanofibrils (BCNFs) fabricated by electron beam irradiation. *Innovative Food Science & Emerging Technologies, 94*, Article 103664. https://doi.org/10.1016/j.ifset.2024.103664

Tang, L., Hu, M., Bai, S., Wang, B., Fan, B., Zhang, L., & Wang, F. (2024). Extraction of insoluble soybean fiber by alternating ultrasonic/alkali and its improved superior physicochemical and functional properties. *International Journal of Biological Macromolecules, 263*(Pt 2), Article 130505. https://doi.org/10.1016/j.ijbiomac.2024.130505

Tang, L., Wang, B., Bai, S., Fan, B., Zhang, L., & Wang, F. (2024). Preparation and characterization of cellulose nanocrystals with high stability from okara by green solvent pretreatment assisted TEMPO oxidation. *Carbohydrate Polymers, 324*, Article 121485. https://doi.org/10.1016/j.carbpol.2023.121485

Tang, W., Wang, R., Li, M., Zhang, Q., He, J., Liu, D., … Liu, J. (2024). High-pressure microfluidization enhanced the stability of sodium caseinate-EGCG complex-stabilized fish oil emulsion. *Food Chemistry, 444*, Article 138669. https://doi.org/10.1016/j.foodchem.2024.138669

Usurelu, C. D., Frone, A. N., Oprica, G. M., Raduly, M. F., Ghiurea, M., Neblea, E. I., … Panaitescu, D. M. (2024). Preparation and functionalization of cellulose nanofibers using a naturally occurring acid and their application in stabilizing linseed oil/water Pickering emulsions. *International Journal of Biological Macromolecules, 262*(Pt 1), Article 129884. https://doi.org/10.1016/j.ijbiomac.2024.129884

Uşurelu, C.-D., Frone, A. N., Oprică, G.-M., Raduly, M. F., Ghiurea, M., Neblea, E. I., … Panaitescu, D. M. (2024). Preparation and functionalization of cellulose nanofibers using a naturally occurring acid and their application in stabilizing linseed oil/water Pickering emulsions. *International Journal of Biological Macromolecules, 262*, Article 129884. https://doi.org/10.1016/j.ijbiomac.2024.129884

Wang, J., Lin, M., Shi, L., Zhao, Y., Liu, S., Liu, Z., … Ren, Z. (2024). Characteristics and stabilization of Pickering emulsions constructed using myosin from bighead carp

(Aristichthys nobilis). *Food Chemistry, 456*, Article 140033. https://doi.org/10.1016/j.foodchem.2024.140033

Wang, M., Bu, G., Zhu, T., Liu, J., Li, M., Rashid, M. T., & Han, M. (2024). Effects of enzymatic hydrolysis combined with glycation on the emulsification characteristics and emulsion stability of peanut protein isolate. *Food Research International, 192*, Article 114722. https://doi.org/10.1016/j.foodres.2024.114722

Wang, M., Liu, Q., Zeng, X., Chen, R., Wang, C., Li, M., … Zhang, Y. (2024). Bacterial cellulose nanofibrils for the physical and oxidative stability of fish oil-loaded Pickering emulsions. *Colloids and Surfaces A: Physicochemical and Engineering Aspects, 694*. https://doi.org/10.1016/j.colsurfa.2024.134154

Wang, Y., Huang, Y., Li, H., Luo, Y., Dai, D., Zhang, Y., … Dai, H. (2024). Low gelatin concentration assisted cellulose nanocrystals stabilized high internal phase emulsion: The key role of interaction. *Carbohydrate Polymers, 337*, Article 122175. https://doi.org/10.1016/j.carbpol.2024.122175

Wu, C., McClements, D. J., Ma, B., Lai, Z., Wu, F., Liu, X., & Wang, P. (2024). Composite hydrogels formed from okara cellulose nanofibers and carrageenan: Fabrication and characterization. *International Journal of Biological Macromolecules, 258*(Pt 2), Article 129079. https://doi.org/10.1016/j.ijbiomac.2023.129079

Xiao, Y., Liu, Y., Wang, X., Li, M., Lei, H., & Xu, H. (2019). Cellulose nanocrystals prepared from wheat bran: Characterization and cytotoxicity assessment. *International Journal of Biological Macromolecules, 140*, 225–233. https://doi.org/10.1016/j.ijbiomac.2019.08.160

Xiao, Y., Xu, H., Zhou, Q., Li, W., Gao, J., Liao, X., … Liu, Y. (2023). Influence mechanism of wheat bran cellulose and cellulose nanocrystals on the storage stability of soy protein isolate films: Conformation modification and molecular interaction perspective. *Food Hydrocolloids, 139*, Article 108475. https://doi.org/10.1016/j.foodhyd.2023.108475

Yan, C., Yin, Y., Zhang, S., Luo, G., Xu, Y., Liu, L., … Zhou, X. (2023). Fabrication and characterization of sunflower oil-in-water emulsions stabilized with sunflower stem pith cellulose nanofibril. *International Journal of Biological Macromolecules, 224*, 919–926. https://doi.org/10.1016/j.ijbiomac.2022.10.177

Yan, W., Zhang, M., Zhang, M., Yadav, M. P., Jia, X., & Yin, L. (2022). Effect of wheat bran arabinoxylan on the gelatinization and long-term retrogradation behavior of wheat starch. *Carbohydrate Polymers, 291*, Article 119581. https://doi.org/10.1016/j.carbpol.2022.119581

Zhang, L., Li, X., Xu, X., Song, L., Bi, A., Wu, C., … Du, M. (2024a). Semisolid medium internal phase emulsions stabilized by dendritic-like mushroom cellulose nanofibrils: Concentration effect and stabilization mechanism. *Food Chemistry, 436*, Article 137693. https://doi.org/10.1016/j.foodchem.2023.137693

Zhang, L., Li, X., Xu, X., Song, L., Bi, A., Wu, C., … Du, M. (2024b). Semisolid medium internal phase emulsions stabilized by dendritic-like mushroom cellulose nanofibrils: Concentration effect and stabilization mechanism. *Food Chemistry, 436*, Article 137693. https://doi.org/10.1016/j.foodchem.2023.137693

Zhao, R., Chang, C., He, Y., Jiang, C., Bao, Z., & Wang, C. (2024). Effects of mixing ratio on physicochemical, structural properties and application in lycopene-loaded emulsions of blends of whey protein and pea protein. *Food Chemistry, 463*(Pt 1), Article 141062. https://doi.org/10.1016/j.foodchem.2024.141062

Zhao, Y., Zhang, F., Chen, M., Liu, F., Zheng, B., Miao, W., … Zhou, R. (2024). Cellulose nanofibrils-stabilized food-grade Pickering emulsions: Clarifying surface charge's contribution and advancing stabilization mechanism understanding. *Food Hydrocolloids, 152*. https://doi.org/10.1016/j.foodhyd.2024.109920

Zhong, J., Xie, H., Wang, Y., Xiong, H., & Zhao, Q. (2024). Nanofibrillated cellulose derived from rice bran, wheat bran, okara as novel dietary fibers: Structural, physicochemical, and functional properties. *International Journal of Biological Macromolecules, 273*, Article 132902. https://doi.org/10.1016/j.ijbiomac.2024.132902

Zhou, Q., Lv, S., Wang, W., Zhu, S., Xu, J., Zheng, M., … Xiao, Y. (2024). Remodeling mechanism of gel network structure of soy protein isolate amyloid fibrils mediated by cellulose nanocrystals. *Carbohydrate Polymers, 332*, Article 121919. https://doi.org/10.1016/j.carbpol.2024.121919

Zhou, Y., Feng, C., Hong, H., Luo, Y., Chang, S. K. C., & Tan, Y. (2024). Plastein reaction enhances the emulsifying and rheological properties of silver carp hydrolysates in oil-in-water emulsions. *Food Hydrocolloids, 153*. https://doi.org/10.1016/j.foodhyd.2024.110048

Zhu, J., Wang, H., Miao, L., Chen, N., Zhang, Q., Wang, Z., … Jiang, L. (2023). Curcumin-loaded oil body emulsions prepared by an ultrasonic and pH-driven method: Fundamental properties, stability, and digestion characteristics. *Ultrasonics Sonochemistry, 101*, Article 106711. https://doi.org/10.1016/j.ultsonch.2023.106711

Zhu, J., Zhu, P., Zhu, Y., Ye, Y., Sun, X., Zhang, Y., … Jiang, F. (2024). Surface charge manipulation for improved humidity sensing of TEMPO-oxidized cellulose nanofibrils. *Carbohydrate Polymers, 335*, Article 122059. https://doi.org/10.1016/j.carbpol.2024.122059